Fractional-Order Control on PX4 Firmware: Open-Source Implementation for Fully-Actuated Hexa-Rotors

Andrés Montes de Oca
Department of Biological and Agricultural Engineering, UC Davis, Davis, CA 95616, USA

Alejandro Flores
Stemmer-Imaging, Queretaro, Qro 76090, Mexico

Aldo Muñoz-Vázquez, Senior Member, IEEE
Department of Multidisciplinary Engineering, Texas A&M University, McAllen, TX 78504, USA

Gerardo Flores, Senior Member, IEEE
School of Engineering, College of Arts and Sciences, Texas A&M Int. University, Laredo, TX 78041 USA

***Abstract*— This paper presents a fractional-order controller for the fully-actuated Hexa-rotor under external disturbances applied to the position and attitude dynamics. We proved that the closed-loop system equilibrium point for the positioning subsystem is globally exponentially stable. Furthermore, the controller provides extraordinary robustness to the system when affected by exogenous and aggressive disturbances. The system's stability is also validated through MATLAB and software in the loop simulations. One of the paper's contributions, apart from the control design, is the implementation of the controller in the PX4 firmware, the most popular open-source autopilot code used worldwide for flying drones. The code is available for download and implemented in real drones. Finally, we have implemented the control algorithm in the PX4-firmware alongside a virtual environment in Gazebo and compared it with the standard PX4-firmware controller. The results considerably outperform the standard PID controller programmed in the PX4 firmware.**

***Index Terms*— Fractional-order control, Fully-actuated, Hexa-rotor, UAV.**

(Corresponding author: G. Flores, e-mail: gerardo.flores@tamu.edu).

A. Montes de Oca is with the Department of Biological and Agricultural Engineering, UC Davis, Davis, CA 95616, USA (e-mail: amoreb@ucdavis.edu). A. Flores is with Stemmer-Imaging, Queretaro, Qro 76090, Mexico (e-mail: a.flores@stemmer-imaging.com). A. Muñoz-Vázquez is with the Department of Multidisciplinary Engineering, Texas A&M University, McAllen, TX 78504, USA (e-mail: aldo.munoz-vazquez@tamu.edu). G. Flores is with the School of Engineering, College of Arts and Sciences, Texas A&M Int. University, Laredo, TX 78041 USA (e-mail: gerardo.flores@tamu.edu)

I. INTRODUCTION

In recent years, the research community has increasingly focused on addressing the problem of disturbance robustness in Unmanned Aerial Vehicles (UAVs) using robust control techniques such as sliding mode control [1]. Notably, these control strategies have predominantly employed integer-order approaches [2]. However, due to the coupling between attitude and position dynamics in UAV systems, and the presence of external disturbances, integer-order controllers often face challenges in achieving effective control [3].

In contrast, fractional-order controllers offer greater flexibility and superior disturbance rejection capabilities compared to their integer-order counterparts [4], [5]. Moreover, fractional-order controllers significantly enhance robustness against modeling uncertainties and system parameter variations by efficiently adapting to dynamic changes and compensating for these uncertainties [4].

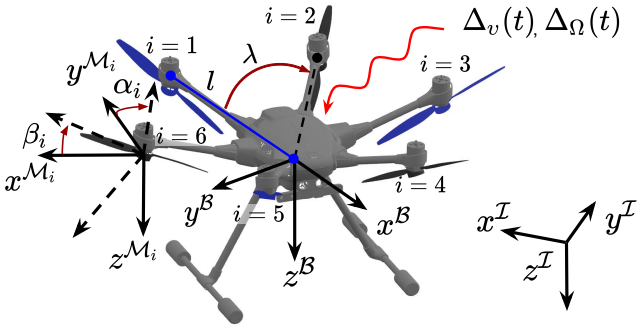

Fig. 1: Coordinate frames $\mathcal{I}$, $\mathcal{B}$, and $\mathcal{M}_i$ of the hexa-rotor UAV. All motors are positioned at a distance l from the UAV's center and are tilted at fixed angles: $\beta = -25°$, $\alpha = 35°(-1)^i$, and $\lambda = 60°$. Here, $i = \{1, 2, \ldots, 6\}$ indexes the i-th motor. Disturbances $\Delta_v(t)$ and $\Delta_\Omega(t)$ affect the translational and rotational dynamics, respectively.

A. STATE OF THE ART

Standard fractional-order sliding mode controls (FOSMC) have been extensively developed for quadrotor UAVs, as demonstrated in [5]–[12], to achieve robust behavior under external disturbances. Furthermore, similar approaches for FOSMCs based on the backstepping method are proposed in [13], [14]. A notable variant of FOSMC is introduced in [15], leveraging an event-trigger-based strategy. The integration of fractional-order controls with PI structures is explored in [16], where a fractional-order integral is combined with sliding mode control. Additionally, fractional-order PID controllers have been shown to enhance system response, as illustrated in [17], with the derivative action improving overall control performance. Similarly, a fractional-order linear active disturbance rejection control scheme is presented in [18], combining the benefits of fractional-order PID and linear active disturbance rejection techniques.

Moreover, fractional nonlinear control strategies, such as those proposed in [19], utilize nested saturations to maintain desired position and orientation during stationary flight and trajectory tracking tasks. Notably, fractional-order control is not limited to quadrotor UAVs; it is also applied to other vehicles, including fixed-wing aircraft. For example, [20], [21] introduce a finite-time fault-tolerant control strategy using a fractional-order backstepping iterative design for fixed-wing platforms.

Despite these advancements, fractional-order control for fully-actuated multi-rotor configurations remains a relatively new research topic, particularly when implemented in autopilot systems. The lack of such controls applied to fully-actuated Hexa-rotor platforms underscores the novelty of this work. To provide context, Table I summarizes recent works employing other techniques aimed at developing robust control strategies.

B. Contribution

We propose a robust position controller for the fully-actuated Hexa-rotor, utilizing a fractional-order integral, as depicted in Fig. 2. The proposed control algorithm guarantees globally exponential stability of the tracking error equilibrium, demonstrating strong robustness through both theoretical stability analysis and realistic software-in-the-loop (SITL) simulations.

To further contribute to the UAV and control community, we have provided open-source code for seamless integration into the PX4 firmware. This includes the implementation of the fractional-order integral in C++, which has been integrated into the PX4 framework. Our fractional-order control implementation outperforms the default PID controller in the PX4 firmware, which is currently the most widely used open-source autopilot code for UAVs. A thorough comparison between our controller and the PX4 default controller validates the superior performance of the proposed approach.

All the developed code, along with comprehensive documentation, is publicly available in our GitHub repository:
https://github.com/andresmr13/Hexarotor_fractional_control_for_PX4.git.
This implementation can be tested using the fully actuated Hexa-rotor model in a virtual environment, as illustrated in Fig. 6, or deployed on a real multi-rotor platform.

C. Outline

The structure of this paper is as follows: Section II introduces the problem to be addressed, including the necessary preliminaries and the mathematical model of the system. Section III presents the proposed control law along with the corresponding theorems and proofs. Section IV details the numerical simulations used to implement the control law and evaluates its performance against state-of-the-art control strategies. Finally, Section V provides a concise summary of the results achieved and outlines potential directions for future research.

Nomenclature

(α_i, β_i) Tilted angles of the motors w.r.t. $\mathcal{B}$
$\Delta_v(t), \Delta_\Omega(t) \in \mathbb{R}^3$ Exogenous unknown disturbances affecting the position and orientation dynamics, respectively
$\hat{e}_3 = [0,\ 0,\ 1]^\intercal$ Basis vector for z direction
$\mathcal{B}$ Hexa-rotor body frame
$\mathcal{I}$ Hexa-rotor inertial frame
$\mathcal{M}_i$ Body frame of i-th motor, $i = \{1, 2, ..., 6\}$
$\Omega = [\omega_x,\ \omega_y,\ \omega_z]^\intercal \in \mathbb{R}^3$ Hexa-rotor's angular rate
$\mu = [\mu_x,\ \mu_y,\ \mu_z]^\intercal \in \mathbb{R}^3$ Torque vector considered as control input for the position dynamics Σ
g Gravity constant
$J \in \mathbb{R}^{3\times3}$ Hexa-rotor's inertia matrix
m Hexa-rotor mass
$p = [x,\ y, z]^\intercal$ Hexa-rotor's position vector in $\mathcal{I}$
$R \in$ SO(3) Rotation matrix from $\mathcal{B}$ to $\mathcal{I}$ representing the Hexa-rotor's orientation
$u_\tau = [u_{\tau_x},\ u_{\tau_y},\ u_{\tau_z}]^\intercal \in \mathbb{R}^3$ Torque vector considered as control input for the attitude dynamics Π
$v = [\dot{x},\ \dot{y},\ \dot{z}]^\intercal$ Hexa-rotor's velocity vector in $\mathcal{I}$

The *hat* map $\hat{(\cdot)} : \mathbb{R}^3 \to \mathfrak{so}(3)$ is defined by $\hat{a}b = a \times b$, $\forall\ a, b \in \mathbb{R}^3$, and then $\hat{\Omega} \in \mathfrak{so}(3)$ is the skew-symmetric matrix of Ω; the inverse of the hat map is the *vee* map $(\cdot)^\vee : \mathfrak{so}(3) \to \mathbb{R}^3$.

II. PROBLEM FORMULATION

A. Preliminaries

DEFINITION 1 (The Riemann–Liouville fractional differ-integral, [26], [27]) *Consider the real-valued function $f(x)$. The Riemann-Liouville fractional derivative is defined by,*

$$ {}_aD_x^\alpha f(x) = \frac{1}{\Gamma(n-\alpha)} \frac{d^n}{dx^n} \int_a^x \frac{f(t)}{(x-t)^{\alpha+1-n}} dt \qquad (1) $$

where a, x are the lower and upper limits, respectively; $n \in \mathbb{N}$, $(n-1 < \alpha < n)$, and $\Gamma(z)$ is the gamma function defined by,

$$ \Gamma(z) = \int_0^\infty \tau^{z-1} e^{-\tau} d\tau. $$

And the Riemann-Liouville fractional integral is defined by,

$$ {}_aD_x^{-\alpha} f(x) = {}_aI_x^\alpha f(x) = \frac{1}{\Gamma(\alpha)} \int_a^x (x-t)^{\alpha-1} f(t) dt. \quad (2) $$

B. Mathematical model

The Hexa-rotor has six fixed tilted motors as shown in Fig. 1, numbered clockwise as $i = 1, 2, 3, 4, 5, 6$. In addition, each motor is tilted at specific angles (α_i, β_i), which determine the orientation of the motor frame $\mathcal{M}_i$ relative

TABLE I: The relevant state-of-the-art of fully-actuated Hexa-rotor control. GES, LES, and GAS mean globally exponentially stable, locally exponentially stable, and globally asymptotically stable, respectively.

Literature	Consider disturbance	Stability achieved	Code released	Method
Our research	✓	GES in attitude and position	✓	Fractional-order control
[22]	✓	GES in attitude and position	✗	Nonlinear model predictive control
[23]	✓	GES in attitude and position	✗	Feedback linearization
[24]	✓	GAS in attitude and position	✗	Adaptive sliding mode control
[25]	✓	Ultimate boundedness stability	✗	Feedback linearization

to the Hexa-rotor body frame $\mathcal{B}$. The mathematical model in the 6-DOF of the Hexa-rotor is as follows, [28]:

$$\Sigma: \begin{cases} \dot{p} = v & \text{(3a)} \\ \dot{v} = g\hat{e}_3 - \dfrac{1}{m} R\mu + \Delta_v(t) & \text{(3b)} \end{cases}$$

$$\Pi: \begin{cases} \dot{R} = R\hat{\Omega} & \text{(4a)} \\ \dot{\Omega} = -J^{-1}\left(\Omega \times J\Omega\right) + J^{-1}u_\tau + \Delta_\Omega(t). & \text{(4b)} \end{cases}$$

The structure of the control input vector in (3b) is $\mu = (\mu_1,\ \mu_2,\ \mu_3)^\intercal$, [29], which opens up the possibility of having a component of the total thrust in the $x-y$ plane, even when $R = I_{3\times 3}$, i.e., when the aerial robot is in hover flight mode. On the other hand, for conventional Hexa-rotors where all the rotors point upwards, the input control vector has a fixed structure $\mu = (0,\ 0,\ T)^\intercal$, where T is the total thrust.

III. MAIN RESULT

To stabilize the dynamics of the fully-actuated Hexa-rotor, it is essential to control the subsystems Σ and Π. In our previous work [30], we successfully addressed the control of the attitude subsystem Π. Building upon that foundation, this paper introduces an enhanced control strategy to reject aggressive exogenous disturbances robustly. The proposed approach consists of two main components: an attitude control law to stabilize the error dynamics of subsystem Σ and a fractional-order position controller to stabilize the error dynamics of subsystem Π. The fractional-order controller represents the core contribution of this work, significantly improving the performance over previous designs.

A. Attitude control

THEOREM 1 (Attitude Controller) *Consider the attitude system Π in (4). And let us define the errors related to attitude dynamics by [31]:*

$$\begin{aligned} e_R &= \frac{1}{2}\left(R_{e,r} - R_{e,r}^\intercal\right)^\vee = [e_R(1),\ e_R(2),\ e_R(3)]^\intercal, \\ e_\Omega &= \Omega - R_{e,r}^\intercal \Omega_d = [e_\Omega(1),\ e_\Omega(2),\ e_\Omega(3)]^\intercal, \\ \Psi_{SO(3)} &= \frac{1}{2}\operatorname{Tr}(I_{3\times 3} - R_{e,r}), \end{aligned} \tag{5}$$

where the right attitude error is $R_{e,r} = R_d^\intercal R$, where R_d is the reference angular position, and $I_{3\times 3}$ is the identity matrix of dimension 3. Then, the control law

$$\begin{aligned} u_\tau = &-J\left(k_R e_R + k_\Omega e_\Omega + k_3 v_R + k_4 v_\Omega\right) + \Omega \times J\Omega \\ &- J(\hat{\Omega} R_{e,r}^\intercal \Omega_d - R_{e,r}^\intercal \dot{\Omega}_d). \end{aligned} \tag{6}$$

with vector signals

$$\begin{aligned} v_R &= \begin{bmatrix} |e_R(1)|^{1/2}\operatorname{sgn} e_R(1) \\ |e_R(2)|^{1/2}\operatorname{sgn} e_R(2) \\ |e_R(3)|^{1/2}\operatorname{sgn} e_R(3) \end{bmatrix}, \\ v_\Omega &= \begin{bmatrix} |e_\Omega(1)|^{1/2}\operatorname{sgn} e_\Omega(1) \\ |e_\Omega(2)|^{1/2}\operatorname{sgn} e_\Omega(2) \\ |e_\Omega(3)|^{1/2}\operatorname{sgn} e_\Omega(3) \end{bmatrix} \end{aligned} \tag{7}$$

exponentially stabilizes the zero equilibrium points (5).

Proof: The proof of this result can be seen in our previous contribution [30]. ■

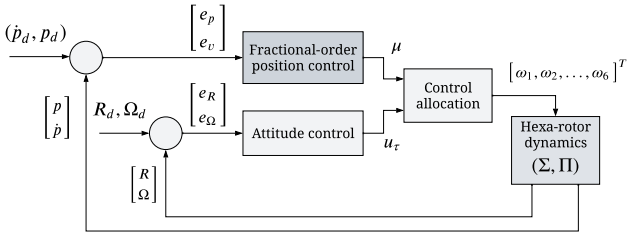

Fig. 2: Block diagram of the proposed fractional-order control.

B. Position control

For the fully-actuated Hexa-rotor position dynamics Σ, we define the error vectors given by,

$$e_p = p - p_d, \qquad e_v = v - \dot{p}_d, \tag{8}$$

where p_d is the desired position trajectory and $(\dot{p}_d, \ddot{p}_d)$ are their the first and second time-derivatives, respectively. They are computed analytically, when possible, or even using advanced differentiator techniques to mitigate the problem of noisy signal derivatives, [32].

Before presenting our main result, let us consider the following assumption.

ASSUMPTION 1 *The external disturbances in system (Σ, Π) are bounded as follows,*

$$\|\Delta_v(t)\|_2 \leq \rho_1 \|I^\alpha s\|_2, \qquad \|\Delta_\Omega(t)\|_2 \leq \rho_2 \|e_\Omega\|, \tag{9}$$

where s is defined in (13), $(\|\cdot\|_2)$ is the Euclidean norm, and $\rho_1, \rho_2 \in \mathbb{R}_{>0}$.

We are ready to present the main result in the following theorem.

THEOREM 2 (Main result: Position Controller Design) *Consider that system Σ satisfies Assumption 1. Also consider the fractional-order integral operator I^α defined in (2). Then, the fractional control law,*

$$-\frac{1}{m}R\mu = -K_1|I^\alpha s|\cdot\frac{s}{|s|} - K_2 s - g\hat{e}_3 + \ddot{p}_d - \Lambda e_v \quad (10)$$

and fractional-order differential equation,

$$\dot{s} = -K_1|I^\alpha s|\cdot\frac{s}{|s|} - K_2 s \quad (11)$$

where $\alpha \in (0,1)$, $(K_1, K_2, \Lambda) \in \mathbb{R}^{3\times 3} \succ 0$, globally exponentially stabilizes the error equilibrium point (8).

Proof: Let us begin by computing the first-time derivatives of the error vectors in (8) by,

$$\begin{aligned}\dot{e}_p &= e_v\\ \dot{e}_v &= g\hat{e}_3 - \frac{1}{m}R\mu + \Delta_v(t) - \ddot{p}_d.\end{aligned} \quad (12)$$

Now, we propose the following sliding surface $s \in \mathbb{R}^3$,

$$s = e_v + \Lambda e_p = [s_1,\ s_2,\ s_3]^\intercal \quad (13)$$

whose time-derivative along the solutions of (12) is computed as,

$$\dot{s} = g\hat{e}_3 - \frac{1}{m}R\mu + \Delta_v(t) - \ddot{p}_d + \Lambda e_v. \quad (14)$$

Now, we are ready to proceed with the stability analysis [33]. Let us consider the candidate Lyapunov function $V = s^\intercal P s$ with $P \succ 0$ whose time-derivative along the solutions of (14) is given by,

$$\begin{aligned}\dot{V} &= \dot{s}^\intercal P s + s^\intercal P \dot{s}\\ &= \left(g\hat{e}_3 - \frac{1}{m}R\mu + \Delta_v(t) - \ddot{p}_d + \Lambda e_v\right)^\intercal P s\\ &\quad + s^\intercal P\left(g\hat{e}_3 - \frac{1}{m}R\mu + \Delta_v(t) - \ddot{p}_d + \Lambda e_v\right).\end{aligned} \quad (15)$$

By equating the previous equation with (14), assuming that the disturbance $\Delta_v(t)$ is unknown, and solving for $-\frac{1}{m}R\mu$, we get the control law defined in (10). We then substitute (10) in (15) to get,

$$\begin{aligned}\dot{V} &= \left(-\left(|I^\alpha s|\cdot\frac{s}{|s|}\right)^\intercal K_1^\intercal - s^\intercal K_2^\intercal + \Delta_v(t)^\intercal\right) P s\\ &\quad + s^\intercal P\left(-K_1\left(|I^\alpha s|\cdot\frac{s}{|s|}\right) - K_2 s + \Delta_v(t)\right)\\ &= -\left(|I^\alpha s|\cdot\frac{s}{|s|}\right)^\intercal K_1^\intercal P s - s^\intercal P K_1\left(|I^\alpha s|\cdot\frac{s}{|s|}\right)\\ &\quad - s^\intercal K_2^\intercal P s - s^\intercal P K_2 s + \Delta_v(t)^\intercal P s + s^\intercal P \Delta_v(t).\end{aligned} \quad (16)$$

For simplicity, consider

$$\frac{|I^\alpha s|}{|s|} = \gamma. \quad (17)$$

The fractional integral operator I^α, with $0 < \alpha < 1$, satisfies norm bounds given by $\|I^\alpha s\| \le C_\alpha \|s\|$, where C_α is a constant that depends on the order α of the operator and the norm space of the function s. These bounds reflect the smoothing nature of fractional integrals, often reducing the magnitude of the original function by attenuating its high-frequency components. This implies $\frac{\|I^\alpha s\|}{\|s\|} \le C_\alpha$, which holds for suitable functions s in spaces like $L^p(\mathbb{R})$ under integrability conditions. Therefore, (16) can be simplified as

$$\begin{aligned}\dot{V} &= -2s^\intercal P K_1 \gamma s\\ &\quad - s^\intercal\left(K_2^\intercal P + P K_2\right) s + 2\Delta_v(t)^\intercal P s.\end{aligned} \quad (18)$$

Since K_2 and P are positive definite, one can find a solution for $K_2^\intercal P + P K_2 = Q$ such that $Q \succ 0$. Also, consider the first inequality of Assumption 1. Then, it follows that

$$\begin{aligned}\dot{V} &\le -s^\intercal\left(2\gamma P K_1 + Q\right) s + 2\rho_1\|I^\alpha s\|\|P s\|\\ &\le -2\gamma s^\intercal P K_1 s - s^\intercal Q s + 2\rho_1\gamma\frac{\sqrt{\lambda_{\max}\{P\}}}{\sqrt{\lambda_{\min}\{P\}}}V\end{aligned} \quad (19)$$

where we have used the eigenvalue bound for quadratic forms:

$$\lambda_{\min}\{P\}\|s\|_2^2 \le V \le \lambda_{\max}\{P\}\|s\|_2^2. \quad (20)$$

Using the same idea of (20) and claiming (17), it follows that,

$$\dot{V} \le -\left(2\gamma\frac{\lambda_{\min}\{PK_1\}}{\lambda_{\max}\{P\}} + \frac{\lambda_{\min}\{Q\}}{\lambda_{\max}\{P\}} + 2\rho_1\gamma\frac{\sqrt{\lambda_{\max}\{P\}}}{\sqrt{\lambda_{\min}\{P\}}}\right)V \quad (21)$$

for all $s \neq 0$. Using the inequality $\lambda_{\min}\{P\}\lambda_{\min}\{K_1\} \le \lambda_{\min}\{PK_1\}$ and following simple computations it follows that,

$$\lambda_{\min}\{K_1\} + \frac{1}{2\gamma}\frac{\lambda_{\min}\{Q\}}{\lambda_{\min}\{P\}} > \rho_1\left(\frac{\lambda_{\max}\{Q\}}{\lambda_{\min}\{P\}}\right)^{3/2} \quad (22)$$

and since V is radially unbounded, it follows that s exponentially converges to zero as long as (22) holds, which is easily achieved by properly choosing the matrix gains K_1 and K_2. This implies that the sliding surface (13) is reduced to $\dot{e}_p = -\Lambda e_p$. Thus, it is clear that the error equilibrium point (8) is globally exponentially stable. ■

IV. SIMULATIONS

A. MATLAB Simulink numerical simulations

In this subsection, we detail the results obtained from numerical simulations using MATLAB Simulink using different orders of integration α for the proposed fractional-order control. To compute the fractional-order integral in the position control, we used the FOMCON toolbox [34], which provides a variety of fractional-order differintegral blocks for control applications. We also simulated the PID control algorithm for comparison purposes.

The control allocation problem is solved from the control inputs in u_τ and μ through the following expression [30],

$$\begin{bmatrix} \mu \\ u_\tau \end{bmatrix} = B(\alpha_i, \beta_i, \lambda, l)\mathrm{v}, \tag{23}$$

where $\mathrm{v} = \left[\omega_1^2, \omega_2^2, ..., \omega_6^2\right]^\intercal$ is the motor spinning rate vector and ω_i is the angular velocity of the i-th motor. $B(\cdot)$ is a function that depends on the Hexa-rotor's parameters such as tilting angles (β, α), motor's arm length l, and distance between motors λ.

TABLE II: Parameter values used in the MATLAB simulation.

$g = 9.81$	$\alpha = -0.5$	$k_3 = \mathrm{diag}[30\ 30\ 30]$
$m = 1$	$\Lambda = \mathrm{diag}[7\ 7\ 7]$	$k_4 = \mathrm{diag}[10\ 10\ 10]$
$\hat{e}_3 = [0\ 0\ 1]$	$K_1 = \mathrm{diag}[50\ 50\ 50]$	$k_R = \mathrm{diag}[50\ 50\ 50]$
$J = \mathrm{diag}([1\ 1\ 1])$	$K_2 = \mathrm{diag}[10\ 10\ 10]$	$k_\Omega = \mathrm{diag}[10\ 10\ 10]$
$K_p = \mathrm{diag}[70\ 70\ 70]$	$K_d = \mathrm{diag}[20\ 20\ 20]$	$K_i = \mathrm{diag}[1\ 1\ 1]$

We used the parameter listed in Table II for the simulations. The results obtained from the simulations are shown in Figs. 3, 4, and 5. First, we show the behavior of the UAV position states during the flight envelope in Fig. 3. This figure depicts the position response under a PID control and the fractional-order control using four different integration orders $I^{0.25}, I^{0.5}, I^{0.75}$. Using the PID control, the errors are considerably bigger than the fractional-order control, reaching error values around ± 0.5 meters. For the case of the fractional-order control, we can see that the errors are smaller with maximum error values around ± 0.05 meters. Now in Fig. 4 we depict the attitude states. It can be seen that the states converge to zero with no oscillation for all the controls. This means that the proposed position control does not affect attitude stability. Finally, the position control outputs are plotted in Fig. 5, where one can see the continuity and smoothness of the signals.

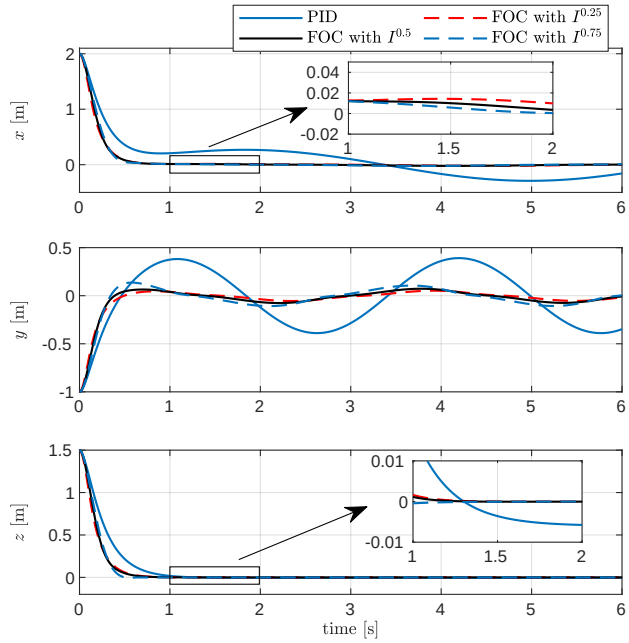

Fig. 3: Position obtained in different simulations varying the fractional-order integration and comparing to the common PID control approach.

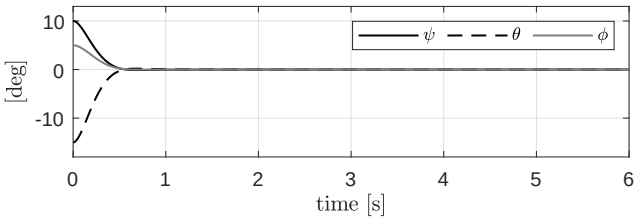

Fig. 4: Attitude states obtained in simulation applying the proposed control approach with fractional-order integration $\alpha = 0.25$.

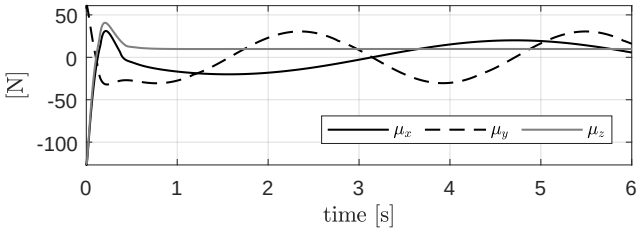

Fig. 5: The proposed fractional-order position control with $\alpha = 0.25$.

B. SITL simulation

In this subsection, we present the implementation of the proposed fractional-order controller in the PX4 firmware through Software in the Loop simulation. These simulations run in a virtual environment in Gazebo, using a 3D model for the fully-actuated Hexa-rotor shown in Fig. 1.

1. *Fractional-order integrator computation*

Since the PX4 firmware is programmed in C++, any control addition should be developed using the same programming language. However, this is a challenging task mainly due to the complex computation of the fractional-order integral. For this reason, we use Oustaloup's method to obtain a numerical approximation. This method uses conventional transfer functions to represent a band-limited approximation of a fractional-order operator. When attempting to approximate a fractional integrator of order

α using a conventional transfer function, it is necessary to calculate the poles and zeros of the transfer function through the use of the following expression, [35]:

$$G_p(\sigma) = \prod_{k=-N}^{N} \frac{\sigma + \omega'_k}{\sigma + \omega_k}, \qquad \omega_k = \left(\frac{b\omega_h}{d}\right)^{\frac{\alpha+2k}{2N+1}}, \quad \omega'_k = \left(\frac{d\omega_b}{b}\right)^{\frac{\alpha-2k}{2N+1}}, \tag{24}$$

where N is the order of approximation in the valid frequency range (ω_b, ω_h), with b, $d \in \mathbb{R}$ as fixed parameters. The transfer function $G_p(\sigma)$ depends on the frequency domain's complex variable σ.

Thus, to make this process practical, the algorithm is decomposed into two steps: 1) compute the continuous-time transfer function of the fractional-order integral and 2) solve its equivalent state-space equations to get the integrated value. Please refer to Algorithm 1 for an overview of the procedures explained next.

The first step is conducted in MATLAB, and the second is conducted through an integrator block in C++. In MATLAB, we create a zero-pole-gain model with the Oustaloup approximation of the fractional-order integrator I^α through (24). Then, the transfer function G_p can be converted to its state-space representation to obtain the state-space matrices (A, B, C, D) as in,

$$\dot{x} = Ax + Bu, \quad y = Cx + Du, \tag{25}$$

where, $A \in \mathbb{R}^{n\times n}$, $B \in \mathbb{R}^{n\times 1}$, $C \in \mathbb{R}^{1\times n}$, and $D \in \mathbb{R}$ are constant and strictly depend on the fractional integration order that is being used in the approximation. The input variable u is the signal to be integrated, defined in (13), and the output variable y is the fractional-order integrated signal equivalent to the $I^\alpha(u)$. Then, we begin with the second step to compute y from the state-space model through C++ in the PX4 firmware. First, we need to take the state-space matrices (A, B, C, D) as constant parameters for the control algorithm. The process for computing a fractional-order integrated value involves first integrating $\dot{x}$ to obtain x, which is then used to compute y. Once y is obtained, it can be used in the fractional control law (10), substituting the term $|I^\alpha s| \cdot \frac{s}{|s|}$. Finally, solving μ from (10) generates control input for the UAV system. Besides, when a different fractional order is utilized, repeating the first step from the outset becomes necessary.

Algorithm 1 Computation of fractional-order integral operator for implementation in the PX4 Firmware.

Require: α, s
Ensure: Fractional-order integral y
Initialize d,b, N, w_b, w_h, k, x, t, t_{prev}, $\dot{x}$, $\dot{x}_{prev}$ with default values.
$w_{kp} \leftarrow (w_h/w_b)^{((k+N+0.5-0.5*\alpha)/(2*N+1))} * w_b$
$w_k \leftarrow (w_h/w_b)^{((k+N+0.5+0.5*\alpha)/(2*N+1))} * w_b$
$K \leftarrow (d * w_h/b)^{\alpha}$
$G_p \leftarrow zpk(-w_{kp'}, -w_{k'}, K) * tf([d, b*w_h, 0], [d*(1-\alpha), b*w_h, d*\alpha])$ ▷ zero-pole-gain form function
$G \leftarrow tf(G_p)$ ▷ convert to transfer function
$A, B, C, D \leftarrow tf2ss(G)$ ▷ convert to state-space
while True **do**
  $u \leftarrow sqrt(|s|) * sgn(s)$ ▷ s from (13)
  $\dot{x} \leftarrow A * x + B * u$
  $y \leftarrow C * x + D * u$ ▷ y is equivalent to $I^\alpha(u)$
  $\Delta t \leftarrow t - t_{prev}$
  $\Delta x \leftarrow (\dot{x} + \dot{x}_{prev}) * \Delta t/2$ ▷ integer-order integration
  $x \leftarrow \Delta x$
  $\dot{x}_{prev} \leftarrow \dot{x}$
  $t_{prev} \leftarrow t$
  $t \leftarrow t + 1$
end while

TABLE III: Parameter values used in the SITL simulation.

$g = 9.81$	$\alpha = -0.5$	$k_3 = \text{diag}[0.2\ 0.2\ 0.2]$
$m = 2.02$	$\Lambda = \text{diag}[1\ 1\ 1]$	$k_4 = \text{diag}[0.01\ 0.01\ 0.01]$
$\hat{e}_3 = [0\ 0\ 1]$	$K_1 = \text{diag}[10\ 10\ 10]$	$k_R = \text{diag}[0.2\ 0.2\ 0.2]$
$J = \text{diag}([0.011\ 0.015\ 0.021])$	$K_2 = \text{diag}[10\ 10\ 10]$	$k_\Omega = \text{diag}[0.06\ 0.06\ 0.06]$
$K_p = \text{diag}[70\ 70\ 70]$	$K_d = \text{diag}[20\ 20\ 20]$	$K_i = \text{diag}[1\ 1\ 1]$

2. *Results*

In the following, we present the results from the software in the loop (SITL) simulation, where the proposed control is programmed into the PX4 firmware and tested in a virtual environment in Gazebo. The fully-actuated Hexa-rotor's virtual model is shown in Fig. 6. The proposed fractional-order control is implemented in the original code using Table III parameters. We present two experiments: hover stabilization and precise trajectory tracking.

The first experiment consists of a hover flight of the Hexa-rotor in the $x = y = 0$ coordinates, achieving an altitude of 2.5 m from the $x = y = z = 0$ position. An external disturbance of $4\sin(0.5t)$ for the x axis and $3\sin(0.1t)$ for the y axis is applied to verify the position controller's performance. We also compare the performance of our fractional-order position controller and the PID controller, commonly used in UAVs and coded by default in the PX4 firmware. This comparison is shown in Fig. 7. It can be seen that the behavior of the UAV while applying the proposed fractional-order control (black line) is considerably more stable than the position with the PID control (red line). In the case of the proposed control, the error obtained does not exceed the 0.2 m in both axes. On the contrary, the PID control does not provide enough robustness against disturbances, with an error reaching more than 1 m and, in certain moments, even 4 m. Finally, Fig. 8 depicts the control signals obtained during the hovering flight applying the proposed control approach. It is observed that the control inputs are continuous and relatively smooth without any chattering effect.

The second experiment is the trajectory tracking. Fig. 9 depicts the position states of the multi-rotor while

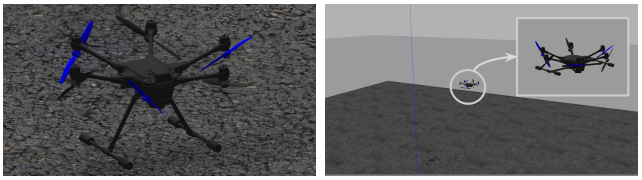

(a) (b)

Fig. 6: a) The fully-actuated Hexa-rotor model in a Gazebo virtual environment. b) Hexa-rotor flying during the SITL experiment.

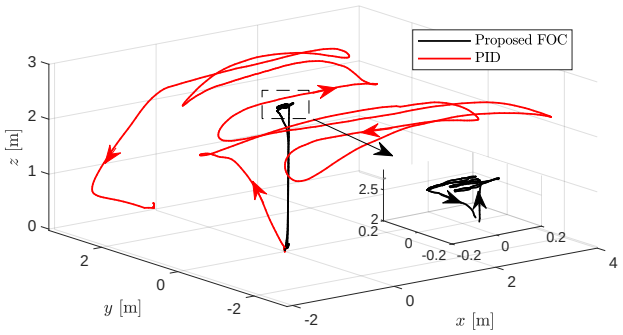

Fig. 7: In SITL simulations, we monitored the position states of the fully-actuated Hexa-rotor. The UAV's position trajectory was visualized with two lines: black for our proposed fractional-order control and red for the standard PID control in PX4 firmware. Analyzing these results provides evidence of our control strategy's advantages.

following a circular-shaped trajectory described by

$$\begin{aligned} x_d(t) &= 4\sin 0.1t, \\ y_d(t) &= 4\cos 0.1t, \\ z_d(t) &= 7.5. \end{aligned} \tag{26}$$

Adding these functions as disturbances to the system makes it easy to observe that the proposed control performs better than the conventional PID. From the same simulation, position errors with the proposed control are depicted in Fig. 10. Since this work's main contribution relies on position control, we only present the attitude results for the fractional-order control simulation to prove that the fully actuated Hexa-rotor does not require to modify its orientation to perform position commands.

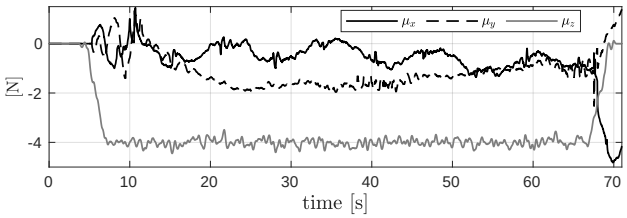

Fig. 8: Fractional-order position control obtained during the SITL simulation of the fully-actuated Hexa-rotor.

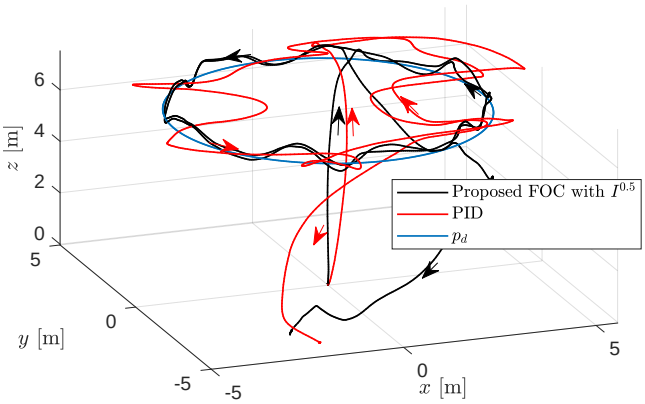

Fig. 9: Position obtained during a SITL simulation performing a circular path tracking between the proposed fractional-order control and the standard PID control approach. The disturbances added to this simulation are defined in (26).

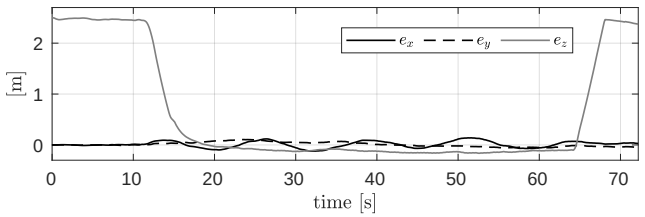

Fig. 10: Hexa-rotor's position errors during the SITL simulation with the fractional-order control and under exogenous disturbances.

This is shown in Fig. 11, where the roll and pitch angles remain low, with values close to zero during the disturbance rejection.

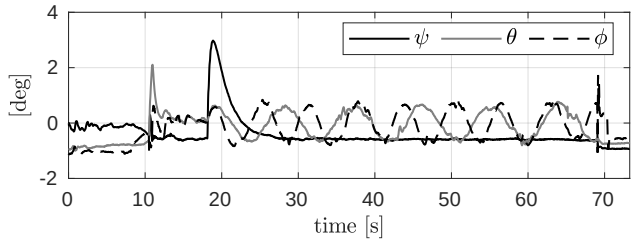

Fig. 11: Hexa-rotor's attitude states during the SITL simulation. It can be seen that the attitude is maintained close to zero regardless of the position control commands. This is possible thanks to the full actuation of the Hexa-rotor.

Additionally, we conduct a performance comparison between different fractional-order values of α in a positioning SITL simulation. Fig. 12 shows the 3D plots of the flights under the FOC with $\alpha = 0.25, 0.5, 0.75$. In the three flight simulations, it is observed that the response is similar with minor errors. For better visualization, we depict the position states (x, y, z) for the three FOC simulations in separate plots in Fig. 13. In this case, it

is easier to see that flight performed using $\alpha = 0.75$ performs the worst from the three simulations while using $\alpha = 0.25$ performs the best.

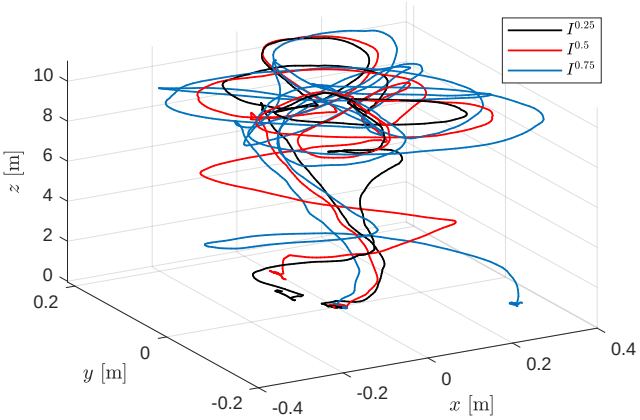

Fig. 12: 3D position obtained during a SITL simulation performing positioning task using three different fractional order values.

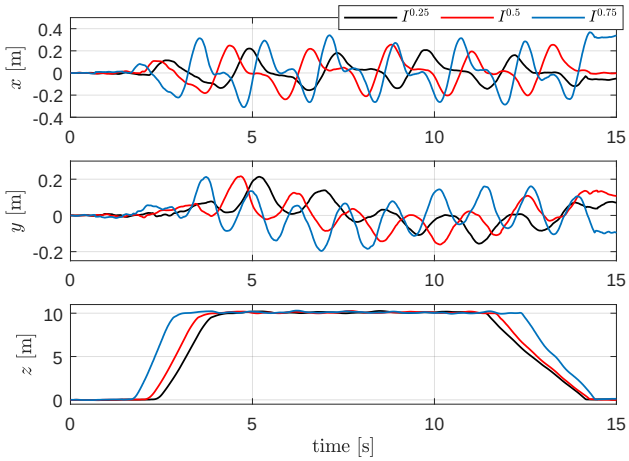

Fig. 13: Axis position obtained during SITL simulations with three different fractional order values.

Finally, we aim to demonstrate that the use of $\dot{p}_d$ and $\ddot{p}_d$ in the control law reduces the error and noise in the path tracking. For that reason, we performed a SITL simulation comparison between the implementation of these terms and those without them. The results can be seen in Fig. 14. In this figure, we depict the position states (x, y) response in two cases: a) using only x_d and b) using $x_d, \dot{p}_d, \ddot{p}_d$. It can be seen that for the second case, the position states are less noisy and close to the reference.

V. CONCLUSIONS

In this research, we have presented the design of a fractional-order control system for the position dynamics of a fully-actuated Hexa-rotor. Our proposed control system is demonstrated to be well-suited for increasing the

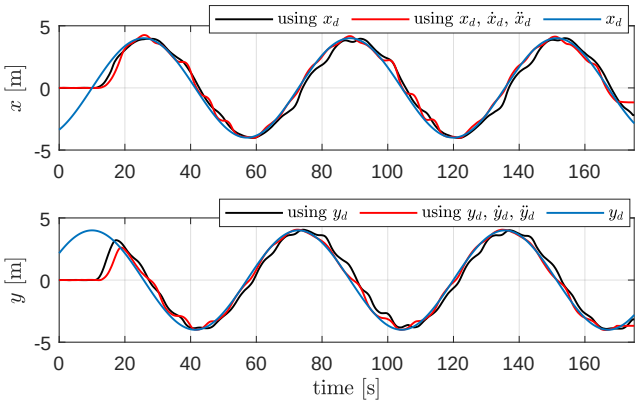

Fig. 14: Path tracking results showing the importance of using $\dot{p}_d$ and $\ddot{p}_d$ terms in the control law.

system's robustness against disturbances. Furthermore, the proposed control law provides global exponential stability to the error equilibrium of the positioning system. Furthermore, we perform MATLAB and software-in-the-loop simulations in a virtual environment using Gazebo to emulate the PX4 firmware in which the control algorithm is programmed. Finally, to demonstrate the superiority of our proposed control system, we also compare it with the performance of the PID control system. Note that PID is the standard controller programmed in the PX4-firmware used for various UAVs worldwide in the drones and robotics communities. The results show that the fractional-order control system is significantly more robust for the position states of the Hexa-rotor than the standard PX4-firmware controller (the PID).

This work comes to enhance our previous results in this research subject: [30], [36]. We plan to conduct real flight experiments using a fully-actuated Hexa-rotor constructed in the lab.

The implemented PX4 code for this paper is available in our GitHub repository, where the reader can find supplementary material.

REFERENCES

[1] H. B. Abebe and C.-L. Hwang
A finite-time trajectory tracking control for a hexa-rotor with uncertainty and actuator fault
In *2022 International Conference on System Science and Engineering (ICSSE)*, 2022, pp. 094–099.

[2] R. Cajo, T. T. Mac, D. Plaza, C. Copot, R. De Keyser, and C. Ionescu
A survey on fractional order control techniques for unmanned aerial and ground vehicles
IEEE Access, vol. 7, pp. 66 864–66 878, 2019.

[3] M. Labbadi and H. E. Moussaoui
An improved adaptive fractional-order fast integral terminal sliding mode control for distributed quadrotor
Mathematics and Computers in Simulation, vol. 188, pp. 120–134, 2021.

[4] M. Dulău, A. Gligor, and T.-M. Dulău
Fractional order controllers versus integer order controllers
Procedia Engineering, vol. 181, pp. 538–545, 2017, 10th International Conference Interdisciplinarity in Engineering (INTER-

ENG) 6-7 October 2016, Tirgu Mures, Romania.

[5] C. Izaguirre-Espinosa, A. J. Muñoz-Vazquez, A. Sanchez-Orta, V. Parra-Vega, and I. Fantoni
Fractional-order control for robust position/yaw tracking of quadrotors with experiments
IEEE Transactions on Control Systems Technology, vol. 27, no. 4, pp. 1645–1650, 2019.

[6] S. Xi, Z. Chen, Z. Chen, and Y. Chen
Trajectory tracking of fractional order quadrotor UAV based on adaptive fuzzy fractional order PID controller
In *2024 14th Asian Control Conference (ASCC)*, 2024, pp. 2054–2059.

[7] K. Saeed Bin Gaufan, S. El-Ferik, and N. M. Alyazidi
Fractional model-based formation control of quad-rotor UAVs using sliding mode backstepping
IEEE Access, vol. 12, pp. 166 460–166 473, 2024.

[8] J. Lavín-Delgado, Z. Zamudio Beltrán, J. Gómez-Aguilar, and E. Pérez-Careta
Controlling a quadrotor uav by means of a fractional nested saturation control
Advances in Space Research, vol. 71, no. 9, pp. 3822–3836, 2023, application of Artificial Intelligence in Tracking Control and Synchronization of Spacecraft.

[9] M. Labbadi and M. Cherkaoui
Adaptive fractional-order nonsingular fast terminal sliding mode based robust tracking control of quadrotor UAV with gaussian random disturbances and uncertainties
IEEE Transactions on Aerospace and Electronic Systems, vol. 57, no. 4, pp. 2265–2277, 2021.

[10] M. Labbadi, Y. Boukal, and M. Cherkaoui
Path following control of quadrotor UAV with continuous fractional-order super twisting sliding mode
Journal of Intelligent and Robotic Systems, vol. 100, 12 2020.

[11] X. Shi *et al.*
Adaptive fractional-order SMC controller design for unmanned quadrotor helicopter under actuator fault and disturbances
IEEE Access, vol. 8, pp. 103 792–103 802, 2020.

[12] C. Hua and J. Chen
Fractional-order sliding mode control of uncertain QUAVs with time-varying state constraints
Nonlinear Dynamics, vol. 95, p. 1347–1360, 01 2019.

[13] M. Vahdanipour and M. Khodabandeh
Adaptive fractional order sliding mode control for a quadrotor with a varying load
Aerospace Science and Technology, vol. 86, pp. 737–747, 2019.

[14] C. Yin, B. Hu, Y. Cheng, J. Xue, and X. Shi
Design of fractional-order backstepping sliding mode controller for the quadrotor unmanned aerial vehicles
In *2018 37th Chinese Control Conference (CCC)*, 2018, pp. 697–702.

[15] M. Pouzesh and S. Mobayen
Event-triggered fractional-order sliding mode control technique for stabilization of disturbed quadrotor unmanned aerial vehicles
Aerospace Science and Technology, vol. 121, p. 107337, 2022.

[16] F. Oliva-Palomo, A. J. Muñoz-Vázquez, A. Sánchez-Orta, V. Parra-Vega, C. Izaguirre-Espinosa, and P. Castillo
A fractional nonlinear PI-structure control for robust attitude tracking of quadrotors
IEEE Transactions on Aerospace and Electronic Systems, vol. 55, no. 6, pp. 2911–2920, 2019.

[17] R. Ayad, W. Nouibat, M. Zareb, and Y. Bestaoui Sebanne
Full control of quadrotor aerial robot using fractional-order FOPID
Iranian Journal of Science and Technology, Transactions of Electrical Engineering, vol. 43, no. 1, pp. 349–360, Jul 2019.

[18] J. Song, Y. Hu, J. Su, M. Zhao, and S. Ai
Fractional-order linear active disturbance rejection control design and optimization based improved sparrow search algorithm for quadrotor UAV with system uncertainties and external disturbance
Drones, vol. 6, no. 9, p. 229, 2022.

[19] J. Lavín-Delgado, Z. Zamudio Beltrán, J. Gómez-Aguilar, and E. Pérez-Careta
Controlling a quadrotor UAV by means of a fractional nested saturation control
Advances in Space Research, vol. 71, no. 9, pp. 3822–3836, 2022.

[20] Z. Yu *et al.*
Refined fractional-order fault-tolerant coordinated tracking control of networked fixed-wing UAVs against faults and communication delays via double recurrent perturbation fnns
IEEE Transactions on Cybernetics, pp. 1–13, 2022.

[21] Z. Yu *et al.*
Nussbaum-based finite-time fractional-order backstepping fault-tolerant flight control of fixed-wing UAV against input saturation with hardware-in-the-loop validation
Mechanical Systems and Signal Processing, vol. 153, p. 107406, 2021.

[22] D. Shawky, C. Yao, and K. Janschek
Nonlinear model predictive control for trajectory tracking of a hexarotor with actively tiltable propellers
In *2021 7th International Conference on Automation, Robotics and Applications (ICARA)*, 2021, pp. 128–134.

[23] G. Michieletto, N. Lissandrini, A. Antonello, R. Antonello, and A. Cenedese
Dual quaternion delay compensating maneuver regulation for fully actuated UAVs
IFAC-PapersOnLine, vol. 53, no. 2, pp. 9316–9321, 2020, 21st IFAC World Congress.

[24] J. M. Arizaga, H. Castaneda, and P. Castillo
Adaptive control for a tilted-motors hexacopter UAS flying on a perturbed environment
In *2019 International Conference on Unmanned Aircraft Systems (ICUAS)*, 2019, pp. 171–177.

[25] A. Baldini, R. Felicetti, A. Freddi, S. Longhi, and A. Monteriu
Disturbance observer based fault tolerant control for tilted hexarotors
In *2021 International Conference on Unmanned Aircraft Systems (ICUAS)*, 2021, pp. 20–27.

[26] Y. Chen, I. Petras, and D. Xue
Fractional order control - a tutorial
In *2009 American Control Conference*, 2009, pp. 1397–1411.

[27] A. Atangana
Chapter 1 - history of derivatives from Newton to Caputo
In *Derivative with a New Parameter*, A. Atangana, Ed. Academic Press, 2016, pp. 1–24.

[28] G. Flores and R. Lozano
Lyapunov-based controller using singular perturbation theory: An application on a mini-UAV
In *2013 American Control Conference*, 2013, pp. 1596–1601.

[29] S. Rajappa, M. Ryll, H. H. Bülthoff, and A. Franchi
Modeling, control and design optimization for a fully-actuated hexarotor aerial vehicle with tilted propellers
In *2015 IEEE International Conference on Robotics and Automation (ICRA)*, 2015, pp. 4006–4013.

[30] G. Flores, A. M. de Oca, and A. Flores
Robust nonlinear control for the fully actuated hexa-rotor: Theory and experiments
IEEE Control Systems Letters, vol. 7, pp. 277–282, 2023.

[31] F. Bullo and A. D. Lewis
Geometric Control of Mechanical Systems. New York, NY, USA: Springer-Verlag New York, 2005.

[32] A. Levant, M. Livne, and X. Yu
Sliding-mode-based differentiation and its application
IFAC-PapersOnLine, vol. 50, no. 1, pp. 1699–1704, 2017, 20th IFAC World Congress.

[33] S. Liu, W. Jiang, X. Li, and X.-F. Zhou
Lyapunov stability analysis of fractional nonlinear systems
Applied Mathematics Letters, vol. 51, pp. 13–19, 2016.

[34] A. Tepljakov, E. Petlenkov, and J. Belikov
Fomcon: Fractional-order modeling and control toolbox for matlab

In *Proceedings of the 18th International Conference Mixed Design of Integrated Circuits and Systems - MIXDES 2011*, 2011, pp. 684–689.

[35] A. Tepljakov *et al.*
Fractional-order modeling and control of ionic polymer-metal composite actuator
Smart Materials and Structures, vol. 28, no. 8, p. 084008, jul 2019.

[36] A. Flores and G. Flores
Fully actuated hexa-rotor UAV: Design, construction, and control. simulation and experimental validation
In *2022 International Conference on Unmanned Aircraft Systems (ICUAS)*, 2022, pp. 1497–1503.